Journal of Hazardous Materials 174 (2010) 299–306

Contents lists available at ScienceDirect

Journal of Hazardous Materials

journal homepage: www.elsevier.com/locate/jhazmat

Characteristics of supported nano-TiO_2/ZSM-5/silica gel (SNTZS): Photocatalytic degradation of phenol

Nor Fauziah Zainudin, Ahmad Zuhairi Abdullah, Abdul Rahman Mohamed*

School of Chemical Engineering, Engineering Campus, Universiti Sains Malaysia, Seri Ampangan, 14300 Nibong Tebal, Penang, Malaysia

ARTICLE INFO

Article history:
Received 17 April 2009
Received in revised form 26 July 2009
Accepted 11 September 2009
Available online 17 September 2009

Keywords:
Photocatalysis
Phenol removal
Supported nano-TiO_2
ZSM-5
Silica gel

ABSTRACT

Photocatalytic degradation of phenol was investigated using the supported nano-TiO_2/ZSM-5/silica gel (SNTZS) as a photocatalyst in a batch reactor. The prepared photocatalyst was characterized using XRD, TEM, FT-IR and BET surface area analysis. The synthesized photocatalyst composition was developed using nano-TiO_2 as the photoactive component and zeolite (ZSM-5) as the adsorbents, all supported on silica gel using colloidal silica gel binder. The optimum formulation of SNTZS catalyst was observed to be (nano-TiO_2:ZSM-5:silica gel:colloidal silica gel = 1:0.6:0.6:1) which giving about 90% degradation of 50 mg/L phenol solution in 180 min. The SNTZS exhibited higher photocatalytic activity than that of the commercial Degussa P25 which only gave 67% degradation. Its high photocatalytic activity was due to its large specific surface area (275.7 m^2/g), small particle size (8.1 nm), high crystalline quality of the synthesized catalyst and low electron–hole pairs recombination rate as ZSM-5 adsorbent was used. The SNTZS photocatalyst synthesized in this study also has been proven to have an excellent adhesion and reusability.

1. Introduction

The presence of harmful organic compounds such as phenols and their derivatives in water supplies and from industrial effluents is an ever increasing problem for the global concern. These organic compounds in the aquatic environment can arise from natural sources such as lignin transformation, hydrolysable tannins and flavanoids, algal secretion and humification processes at low concentration. However, at high concentrations, phenolic compounds can be found in agricultural activities and some industrial wastewater discharges such as coal gasification, resin manufacturing, oil refining, coking plants, chemical synthesis, dyes, plastics, textiles, pharmaceuticals, paper mill, herbicides and fungicides production [1,2].

Due to the high solubility and stability of phenolic compounds in water, it is an onerous process to treat phenolic water to innocuous levels for many biological and chemical processes [3]. Conventional water treatment technologies such as solvent extraction, activated carbon adsorption, and chemical treatment process such as oxidation by ozone (O_3) often produce hazardous by-products and generate large amount of solid wastes, which require costly disposal or regeneration method [4]. Biological treatment is often not convenient for treatment of phenolic wastewater as its toxicity may cause the phytotoxic effect on the active microorganisms [5]. Due to these reasons, considerable attention has been focused on complete oxidation of organic compounds to harmless products such as CO_2 and H_2O by the advanced oxidation process (AOP) that appears to be the most emerging technology recently [6].

A great deal of attention has been devoted to titanium dioxide (TiO_2) especially in nano-sized TiO_2 for use as photocatalyst due to the stability of its chemical structure, high surface area, biocompatibility, physical, nontoxicity, low cost and it possesses high oxidizing power [7–11]. However, from an engineering point of view, the immobilization of nano-TiO_2 onto support is preferable compared to the slurry system as to avoid costly and difficult separation and for the purpose of recycling the photocatalyst [12,13]. Among the various supports, silica gel is the most promising support because of its excellent characteristics in light transmission and adsorption of pollutants [14]. Nevertheless, there are problems that limit the potential of nano-TiO_2 photocatalysis in wastewater treatment. According to Haque et al. [15], major limitations arise from the requirement for near UV light and the fact that the intrinsic quantum yields of titania are low leading to a high-energy requirement to drive lamps.

We attempt to solve these problems by dispersing nano-TiO_2 onto a good adsorbent, since reactions predominantly occur on the surface. The adsorbents concentrate pollutants to the photocatalyst surface, even in the dark, which reduces the requirement of a high-energy [16–18]. Among the various adsorbents, zeolite (ZSM-5) has been chosen for the several reasons: its unique Al–O units in

* Corresponding author. Tel.: +06 045996410; fax: +06 045941013.
E-mail address: chrahman@eng.usm.my (A.R. Mohamed).

0304-3894/$ – see front matter © 2009 Elsevier B.V. All rights reserved.
doi:10.1016/j.jhazmat.2009.09.051

zeolite framework are the photocatalytic active sites, it can delocalize band gap excited electrons of nano-TiO_2, thus, reducing the electron–hole recombination process on the surface and adsorption of the intermediates [19,20].

With this goal in mind, special attention was given in this research in order to obtain the optimum composition of each component in this supported catalyst and to study the reusability of the prepared catalyst. The prepared catalyst consists of a mixture of ZSM-5 and modified nano-TiO_2 which was enriched by Degussa P25 and supported onto the silica gel using colloidal silica gel as binder.

2. Materials and methods

2.1. Materials

Phenol (≥99.5%) was selected as a model organic compound in the present study. It was purchased from Fisher Scientific and used as received. Powdered particles of Zeolite ZSM-5 (425 m^2/g and Si/Al = 23) was purchased from Zeolyst International and calcined at 500 °C for an hour. Silica gel with particle sizes of 0.2–0.5 mm was purchased from Acros Organic. Colloidal silica gel (30 wt.% silica suspension in water) was purchased from the Sigma–Aldrich and used as received. For the preparation of the nano-TiO_2 based catalyst, titanium (IV) isopropoxide (TTIP, 98%) and ethanol (C_2H_5OH 95%) were purchased from the Acros Organic and TiO_2 Degussa P25 powder (50 m^2/g; 15–30% rutile + 85–70% anatase) was purchased from the Degussa, Germany. All the solutions were prepared using deionized water from Milli-Q system and controlled by its resistivity (18.2 MΩ).

2.2. Catalyst preparation

TiO_2 nanoparticle was synthesized using sol–gel method as reported by Gennequin et al. [21]. A mixture of 1 TTIP:$2C_2H_5OH$:$5H_2O$ was prepared for the sol–gel solution. Solution of TTIP in ethanol was prepared and stirred at room temperature for an hour. Subsequently, water was added drop by drop under a vigorous stirring. The gel obtained was dried at 80 °C for 24 h. The modified sol–gel solution was prepared by adding calculated amount of Degussa P25 to the sol solution before drying in an oven at 80 °C for 24 h. The powder was added slowly with vigorous stirring to prevent the formation of agglomerates. The obtained nano-TiO_2 was then immobilized according to the literature method [15]. A known weight of nano-TiO_2 and ZSM-5 were mixed together and dispersed uniformly in the appropriate amount of colloidal silica gel binder. A known weight of silica gel then magnetically stirred into the mixture for 30 min. The mixture was dried at ambient conditions and then dried in an oven at 100 °C. The granules obtained were gently crushed and screened, followed by washing with deionized water for several times. After the completion of the impregnation process, the catalyst was calcined in a furnace at 600 °C for 3 h.

2.3. Catalyst characterization

The X-ray diffraction (XRD) patterns were obtained using a Siemens D5000 powder diffractometer using Cu Kα radiation (40 kV, 30 mA) at a scan rate (2θ) of 0.05°/s. It was also used to determine the identity of any phase present in the sample and their crystalline size. The mass fraction of rutile (W_R) and anatase (W_A) were estimated by measuring the relative intensities of the strongest diffraction peaks of rutile (I_R) and anatase (I_A), respectively, using the following equation [22].

$$W_R = \frac{1.26 I_R}{I_A + 1.26 I_R} \quad (1)$$

The crystallite size can be determined from the broadening of corresponding X-ray spectral peaks by the Scherrer's equation [23]:

$$L = \frac{K\lambda}{\beta \cos\theta} \quad (2)$$

where L is the crystallite size, λ the wavelength of the X-ray diffraction (Cu Kα = 1.5406 Å), K shape factor (usually taken as 0.89) and β the line width at half-maximum height. The particles sizes and shapes were observed using a transmission electron microscopy (TEM) (Philips CM12). The samples for TEM were prepared by dispersing the powder in ethanol. The suspension obtained was dropped on a carbon film coated 400 mesh copper grid and dried at room temperature for at least 15 min. The surface-adsorbed water and hydroxyl groups on the photocatalysts were studied by a Fourier transform infrared spectroscopy (PerkinElmer FT-IR Spectrum 2000 spectrometer, USA) within the range wavenumber of 400–4000 cm^{-1} using KBr pellets. The KBr was grounded into the powders and mixed with the solid samples. Then, pellets were prepared by pressing the powder at 66,000 kPa of pressure using uniaxial press. The background was automatically corrected from the sample spectra by scanning for pure KBr. The Brunauer–Emmett–Teller (BET) surface area and pore size distribution were obtained using a Micromeritics ASAP 2000 (Nocross, GA) nitrogen adsorption apparatus. All the samples were degassed at 180 °C prior to BET measurements.

2.4. Photocatalytic activity measurements

The photocatalytic activities of the prepared catalysts were evaluated in the batch-mode photocatalytic reactor. It consists of a pyrex glass jacketed reactor with dimensions of 23 cm × 10 cm × 8 cm (height × outside diameter × inside diameter) and at the top portion has ports for sampling, gas purging, thermocouple and UV lamp. The lamp and reactor were placed inside a wooden box painted black so that no stray light can enter the reactor. The reactor was placed on a magnetic stirrer for thorough mixing. A low pressure mercury lamp (PCQ lamp, UVP, Inc.) was located at the center of the reactor. It emitted UV light at a wavelength of 254 nm with the maximum intensity of 5400 μW/cm^2. Quartz tube of 1 cm in diameter was used to protect the lamp from any contact with the solution. In order to conduct experiments at the controlled temperature and to protect the lamp from overheating, the reactor was surrounded with a cooling jacket and a fan.

An aqueous suspension of phenol (50 mg/L, 500 mL) containing the required quantity of supported photocatalyst was stirred for about 30 min in the dark to reach the adsorption/desorption equilibrium, followed by UV lamp illumination for the degradation of phenol. During the experiments, air was bubbled into the phenol solutions at a constant flow rate of 2 mL/min. All reaction was carried out in atmospheric pressure and at room temperature. A base supported catalyst, consisting of a mixture of nano-TiO_2 and ZSM-5 supported on silica gel using colloidal silica gel as binder (nano-TiO_2:ZSM-5:silica gel:colloidal silica gel = 1:1:1:2), was used as the reference point in order to evaluate the optimum loading for each of the catalyst component. For a base supported catalyst, 0.25 g TiO_2 was used in 500 mL phenol (0.5 g/L TiO_2). Samples of the suspension were removed at the specific time intervals for analysis. The residual phenol concentration was monitored using a high-performance liquid chromatography (HPLC). The HPLC system used in the experiment comprised of PerkinElmer UV–vis 200 HPLC Detector, a Luna 5 μm C18 (2) 100A column and a PerkinElmer 200 HPLC pump with an injector port. The mobile phase in this HPLC system consisted of 40% acetonitrile and 60% deionized water. The flow rate was adjusted to 1 mL/min. Full loop injection at 20 μL was conducted and the retention time of phenol was 3.81 min. Before HPLC

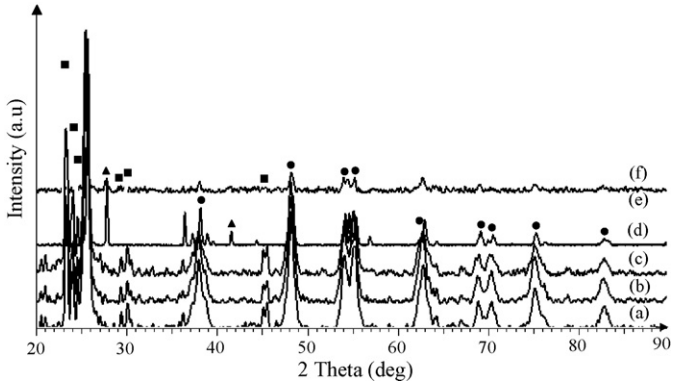

Fig. 1. XRD diffraction pattern of (a) SNTZS (optimum composition) calcined at 600 °C (b) SNTZS (0.9 g/L TiO_2) calcined at 600 °C (c) SNTZS (0.5 g/L) calcined at 600 °C (d) pure nano-TiO_2 calcined at 600 °C (e) fresh SNTZS (optimum composition) and (f) fresh pure nano-TiO_2 (Anatase; Rutile; ZSM-5).

analysis, all samples were filtered using WHATMAN filter (PTFE-membrane, 0.45 μm).

The percentage of phenol remaining, X was calculated using the following equation:

$$X = 100\% - \left(\frac{C_0 - C_t}{C_0}\right) \times 100\%$$

where C_0 is the concentration of phenol at the initial time of zero in mg/L and C_t is the concentration of phenol at time t in mg/L.

3. Results and discussion

3.1. Characterization of the catalysts

The phase structure of fresh and calcined prepared samples were characterized by XRD as shown in Fig. 1. The results of the structural analysis of the catalyst samples as discussed in Section 2.3 have been summarized in Table 1. The findings show that the fresh pure nano-TiO_2 and fresh SNTZS are in the amorphous form in nature. However, the pure nano-TiO_2 calcined at 600 °C comprised both rutile and anatase phase while anatase was the only crystalline phase present in the SNTZS calcined at the same temperature (no rutile and brookite were identified). Therefore, it is reasonable to suggest that an addition of additives changed the temperature of phase transformation from anatase to rutile [22]. The synthesized anatase was more stable compared to that reported in the literatures [24–26] which stating that the transformation of anatase to rutile started at 500–600 °C. This improvement might relate to the interfacial energy effects in anatase TiO_2 and the ZSM-5 (crystalline zeolite), which in turn stabilized the anatase phase. Even the Degussa P25 which containing 15–30% rutile was added in the TiO_2 sol, no rutile peak is appeared in XRD spectra of SNTZS samples. This might be corresponding to the small amount of Degussa P25 loading (10 g/L Degussa P25). The Degussa P25 loading and its rutile ratio in the Degussa P25 composition are too small to be detected in the XRD pattern. Similar result was obtained by Chen et al., 2007. In the case of calcined SNTZS, they had broader peak compared to calcined pure nano-TiO_2. This indicated

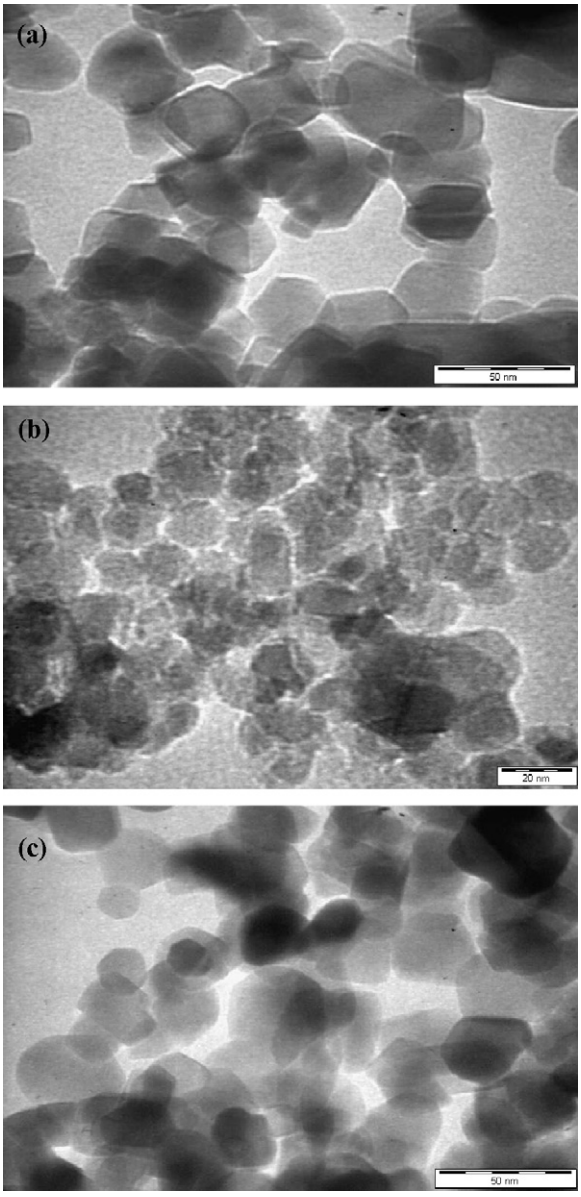

Fig. 2. TEM images of (a) pure nano-TiO_2 powder; (b) SNTZS and (c) Degussa P25.

the formation of smaller crystallite sized calcined SNTZS catalyst. Viswanath and Ramasamy [22] reported that the addition of barrier materials such as organic ligands, porous amorphous polymers or glass, crystalline zeolites, molecular sieve type materials, graphite-type layered materials could control the growth of the crystallites. Fig. 1(b) and (c) reveals that the barrier effect of ZSM-5 successfully control the growth of the TiO_2 crystallite, so that even increase the TiO_2 loading (0.5–0.9 g/L TiO_2) cause the increase in crystallite size as well, but the increase is not too significant (10.6–10.8 nm).

Fig. 2(a–c) shows the TEM images of the calcined pure nano-TiO_2 powder, calcined SNTZS (optimum composition) and Degussa P25, respectively. The average diameters of the particle sizes for the pure

Table 1
Results of the structural analysis of catalysts calculated from XRD data.

Samples	WA (%)	WR (%)	Anatase crystallite size (nm)	Rutile crystallite size (nm)
Pure nano-TiO_2 calcined at 600 °C	70.4	29.6	36.1	20.6
SNTZS (optimum composition) calcined at 600 °C	100.0	–	8.1	–
SNTZS (0.5 g/L TiO_2) calcined at 600 °C	100.0	–	10.6	–
SNTZS (0.9 g/L TiO_2) calcined at 600 °C	100.0	–	10.8	–

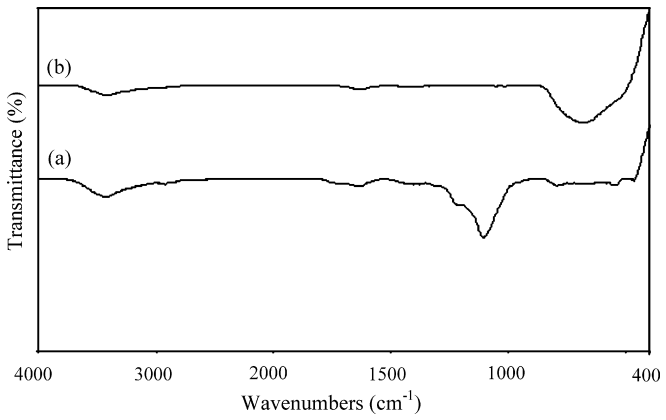

Fig. 3. FT-IR spectra of (a) SNTZS and (b) Degussa P25.

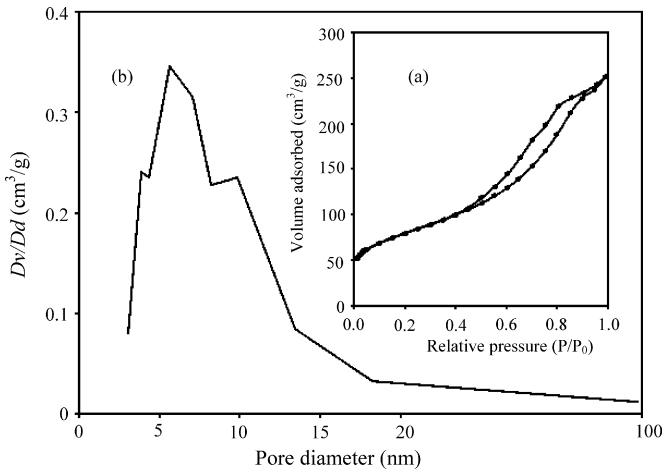

Fig. 4. The nitrogen adsorption–desorption isotherm (a) and Barrett–Joyner–Halenda (BJH) pore size distribution curve (b) calculated from the desorption branch of the nitrogen isotherm of the SNTZS.

nano-TiO_2 and SNTZS were estimated in the range of 20–38 nm and 8–22 nm, respectively. This finding is in agreement with the results measured based on the XRD analysis. The representative image in Fig. 2 reveals that the SNTZS sample consisted of fine particles with homogeneous in size. On the other hand, the TEM analysis shows that the pure nano-TiO_2 was the irregular shaped, consisting of both spherical and polyhedral shapes. Similar to the pure nano-TiO_2, Degussa P25 was spherical and polyhedral shaped with the average particle size of about 21.3 nm.

Fig. 3 depicts the FT-IR spectra of calcined SNTZS (optimum composition) and Degussa P25. The bands at 3429 cm^{-1} and 1630 cm^{-1} represent the surface-adsorbed water and hydroxyl group [27]. This adsorbed water was probably due to humid KBr and incorporated humidity in the process of sample preparation [28]. Based on the research by Okte et al. [29], the peak at wave number near 1102 cm^{-1} can be attributed to the framework stretching vibration band of Si(Al)–O in tetrahedral $Si(Al)O_4$ of raw ZSM-5. In SNTZS spectra, the peak appeared at 1106 cm^{-1} (compared to 1102 cm^{-1}, the peak shifted slightly upward). The broaden peaks of both catalysts within 500–1000 cm^{-1} correspond to Ti–O–Ti linkages in the TiO_2 nanoparticles. It should be noted that the peak for Degussa P25 was more intense than that of the SNTZS. The addition of ZSM-5 in SNTZS resulted in decreasing the intensity of the broad absorption band between 500 cm^{-1} and 1000 cm^{-1}. This finding is supported by the work of Xie et al. [12] which observed that the broad band in the region of 500–1000 cm^{-1} decreased with the addition of silica and disappeared in the case of TiO_2–50% SiO_2, implying that Ti atoms gradually changed from an octahedral environment to a tetrahedral environment as more Ti atoms were incorporated into the tetrahedral sites in the silica network.

Fig. 4(a) shows the nitrogen adsorption–desorption isotherm and (b) the Barrett–Joyner–Halenda (BJH) pore size distribution curve calculated from the desorption branch of the nitrogen isotherm of the calcined SNTZS (optimum composition). The isotherm is of type IV according to the IUPAC classification [30], indicating the presence of mesopores structure of the sample. The hysteresis loop is similar to type H2 which represents a non-uniform size and shape pores. Fig. 4(b) shows that the lower limit of the distribution is 3 nm while the upper limit of the distribution is 18 nm and the pore size distribution is narrow and centered around 5.6 nm. As listed in Table 2, the average pore diameter of SNTZS (optimum composition) decreased compared to the pure nano-TiO_2 due to the presence of ZSM-5 (5.5–6 nm pore diameter). Besides, ZSM-5 acts as a barrier in controlling the growth of nano-TiO_2 crystallites as revealed in XRD results. The pore volume also increased in the presence of the crystalline ZSM-5. It can be seen from Table 2 that the pure nano-TiO_2 possessed the surface area of 11.7 m^2/g. With optimum composition of SNTZS, the specific surface area increased drastically to 275.7 m^2/g, which was five times higher than that of the Degussa P25 (50 m^2/g). This behaviour is for sure very much contributed by the presence of ZSM-5 which it is known that ZSM-5 has pore diameter 5.5–6 nm with a narrow pore volume distribution. That means the SNTZS which possessing the higher surface areas and pore volumes had more surface active sites and channels that allowed the rapid diffusion of various liquid reactants and products during the photocatalytic reaction and thus, increasing the photodegradation rate of reaction [3,31].

3.2. Phenol degradation

The phenol degradation as a model reaction was employed to investigate the photocatalytic activities of the synthesized SNTZS catalyst samples under the UV irradiation. To determine and verify the factors that influencing the photocatalysis, a series of experiments were conducted as the control experiments in 6 h. No appreciable phenol degradation was found in the absence of either UV irradiation, catalyst or air. According to the control experiments without any irradiation, the concentration of phenol decreased less than 6% and 3% due to air stripping and catalyst adsorption, respectively. As for the photolysis of phenol, the concentration of phenol dropped slowly by about 28% of the initial concentration (diagram not shown).

3.3. Optimum composition of SNTZS photocatalyst in degradation of phenol

Selection of optimum catalyst composition is important in order to minimize the excess of catalyst and for economic factor. Thus, each component loaded in the SNTZS was investigated.

Table 2
The textural properties of catalysts.

Samples	BET surface area (m^2/g)	Pore volume (cm^3/g)	Average pore diameter (nm)
Pure nano-TiO_2	11.7	0.022	7.4
SNTZS (optimum composition)	275.7	0.389	5.6
SNTZS (0.5 g/L TiO_2)	247.6	0.406	6.6
SNTZS (0.9 g/L TiO_2)	193.6	0.392	8.1
Degussa P-25	50.0	–	–

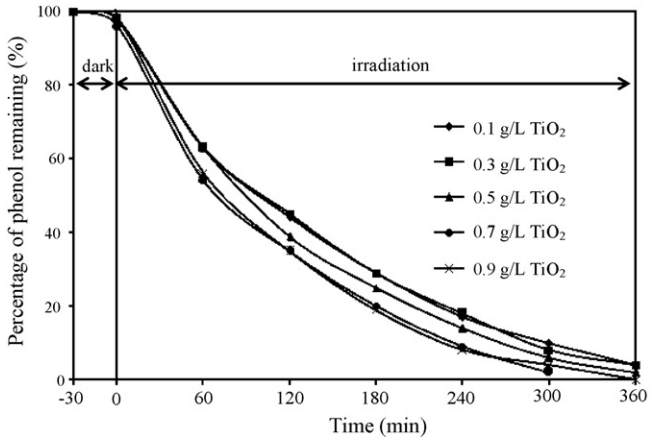

Fig. 5. Degradation of phenol at different nano-TiO_2 loading, based on the base supported catalyst composition (nano-TiO_2:ZSM-5:silica gel:colloidal silica gel = 1:1:1:2) which 0.25 g TiO_2 was used in 500 mL phenol (0.5 g/L TiO_2). *Conditions*: Air flow rate = 2 L/min, initial phenol concentration = 50 mg/L).

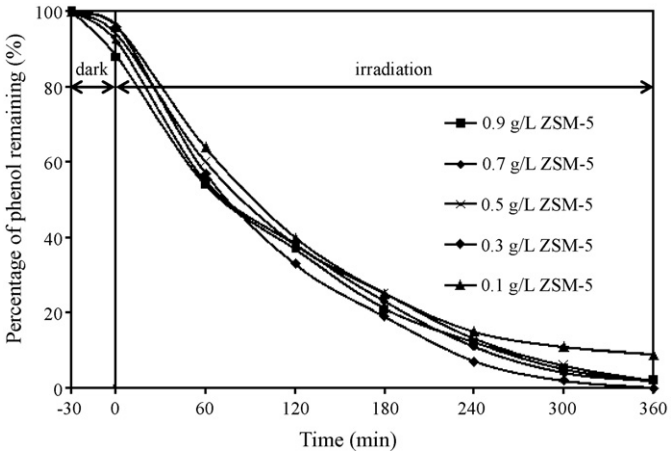

Fig. 6. Degradation of phenol at different adsorbent loading, based on the base supported catalyst composition (nano-TiO_2:ZSM-5:silica gel:colloidal silica gel = 1:1:1:2) which 0.25 g TiO_2 was used in 500 mL phenol (0.5 g/L TiO_2). *Conditions*: Air flow rate = 2 L/min, initial phenol concentration = 50 mg/L.

3.3.1. Nano-TiO_2 loading

Fig. 5 shows the phenol concentration plotted as a function of reaction time over the SNTZS catalyst. For the loadings of nano-TiO_2 in the range of 0.1–0.9 g/L, it was believed that an increase in the nano-TiO_2 loading increased the photodegradation rate owing to the higher holes and hydroxyl radicals generated. However, it remained almost constant beyond certain level as shown in Fig. 5. This performance was due to the fact that the numbers of photons absorbed and the number of phenol molecules adsorbed were increased with increasing the amount of nano-TiO_2 loaded. After above a certain level, TiO_2 particles were in excess. The use of higher amounts of nano-TiO_2 (over 0.5 g/L nano-TiO_2) has been found not to show the significant phenol removal. This is due to the increased light scattering and consequently reduction of the UV light penetration through the solution (the UV light penetration was hindering by excess catalyst particles) [32,33]. Besides, as the nano-TiO_2 loading increased, it could provoke the extensive aggregation of nano-TiO_2 particles on the catalyst surface. Hence, the specific surface areas of the catalyst were reduced and consequently reducing the photodegradation efficiency. This statement was proven by the BET results in which the surface area of the catalyst over 0.5 g/L was reduced from 247.6 m^2/g (0.5 g/L nano-TiO_2) to 193.6 m^2/g (0.9 g/L nano-TiO_2).

3.3.2. Adsorbent loading

The composition of ZSM-5 loading was varied from 0.1 g/L to 0.9 g/L. Fig. 6 shows that 0.3 g/L of ZSM-5 exhibited the optimum adsorbent loading. 0.9 g/L of adsorbent loading shows more pronounced activity in the first 60 min irradiation time, indicating that higher interaction between the preadsorbed phenol molecules and incoming molecule, yielding more occupancy of the available surface area [34]. For the first 30 min in the dark condition, increasing the ZSM-5 loading led to increasing the phenol degradation. After the illumination of UV lamp, photodegradation takes place which indicates that the increase in the addition of ZSM-5 over 0.3 g/L did not affect the degradation of phenol significantly. An increase in the photocatalytic activities was due to the higher adsorption area towards the organic substrates, in turn, making the organic molecules accessible to the active sites on the nano-TiO_2 surface. Degradation of phenol was slower for high surface ZSM-5, thus, increasing the diffusion pathway for phenol molecules [35]. Fig. 7 shows the schematic diagram depicting the heterogeneous nano-TiO_2 photocatalysis process [36–38].

3.3.3. Support loading

Fig. 8 illustrates the effects of different support loadings (0.1–0.9 g/L) on the degradation of phenol. The adsorption of phenol on the catalyst in the dark condition increased with increasing the silica gel content in the catalyst. However, under the illumination, an increase in the silica gel loading led to the improvement of the phenol degradation until it reaches an optimum silica gel level at 0.3 g/L. Further addition of silica gel reduced the phenol degradation as silica gel possessed the adsorption ability for the

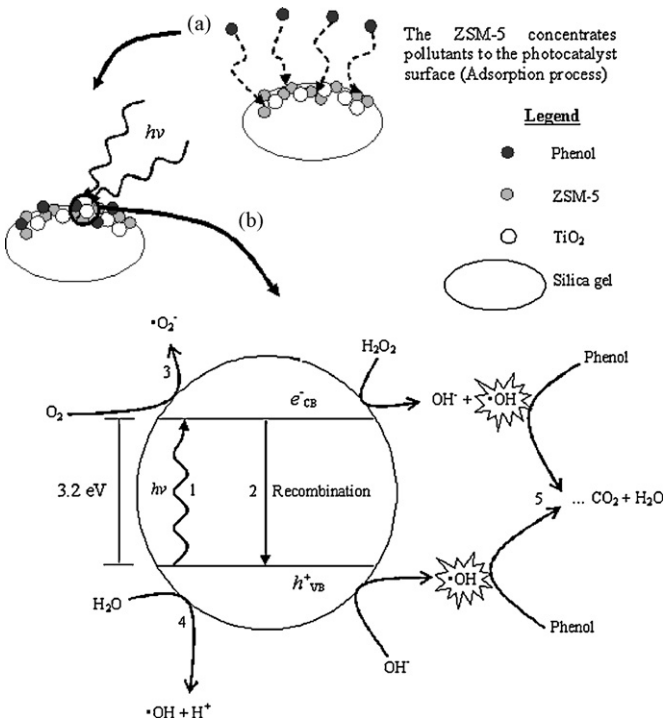

Fig. 7. Schematic representation of (a) ZSM-5 concentrates pollutants to the photocatalyst surface (Adsorption process) and (b) mechanism of photocatalytic activity involving (1) absorption of photon and electron–hole pair generation. The electrons are excited from valence band (VB) to conduction band (CB). In (2), the arrow shows the recombination of electron–hole either on the surface or in the bulk volume. The photogenerated electrons can reduce an electron acceptor (3) and the photogenerated holes can oxidized an electron donor (4). Chain of reactions involved in the production of reactive oxygen species such as H_2O_2, $\bullet O_2^-$ and hydroxyl radical ($\bullet$OH) which eventually mineralizing phenols to CO_2 and water (5).

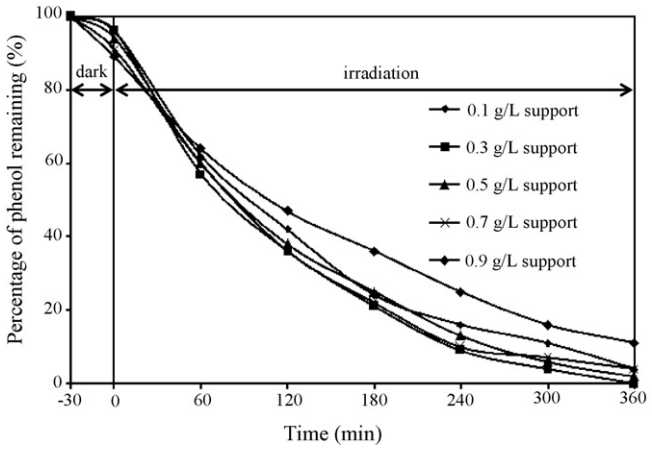

Fig. 8. Degradation of phenol at different support loading, based on the base supported catalyst composition (nano-TiO_2:ZSM-5:silica gel:colloidal silica gel = 1:1:1:2) which 0.25 g TiO_2 was used in 500 mL phenol (0.5 g/L TiO_2). *Conditions*: Air flow rate = 2 L/min, initial phenol concentration = 50 mg/L).

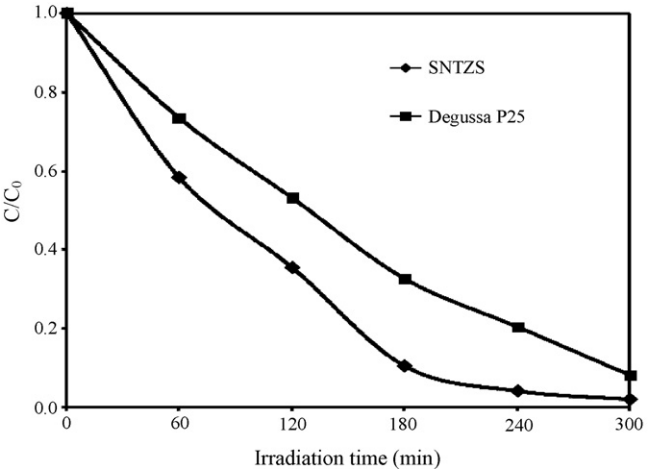

Fig. 10. Photocatalytic activity of synthesized SNTZS and commercial Degussa P25, based on the optimum supported catalyst composition (nano-TiO_2:ZSM-5:silica gel: colloidal silica gel = 1:0.6:0.6:1) which 0.25 g TiO_2 was used in 500 mL phenol (0.5 g/L TiO_2). Degussa P25 in the amount of 0.25 g TiO_2 was also used in 500 mL phenol (0.5 g/L, TiO_2). *Conditions*: Air flow rate = 2 L/min, initial phenol concentration = 50 mg/L).

contaminant [14]. This is also consistent with the earlier finding which indicates that an increase in the adsorption will lead to a decrease in the photocatalytic degradation.

3.3.4. Binder loading

One of the approaches to immobilize the photocatalyst is using a binding method. The important requirement for a binder is it must possess a good adherence between the catalyst and support over a prolonged period of time without losing its photocatalytic activity. According to the studies reported by Haque et al. [15], colloidal silica gel binder exhibits the best contaminant degradation efficiency and high long-term stability. The synthesized SNTZS in this work can be easily recovered from the degraded phenol solution by a simple filtration method and reused without any pretreatment. In order to study the effectiveness of the binder loading, the effect of the reused SNTZS on the photocatalytic activity was investigated. Fig. 9 demonstrates the reusability of the prepared catalyst on different amounts of colloidal silica gel binder (0.5–1.5 g/L) obtained after four experimental runs. After each run, it was observed that the color of the SNTZS turned to dark brown. The change in color of photocatalyst was due to the accumulation of intermediates on the active sites of TiO_2 surface [39], hence, attributing to the reduction of the photocatalytic activity of the reused catalyst. The result in Fig. 9 shows that the decrease in percentage of degradation was

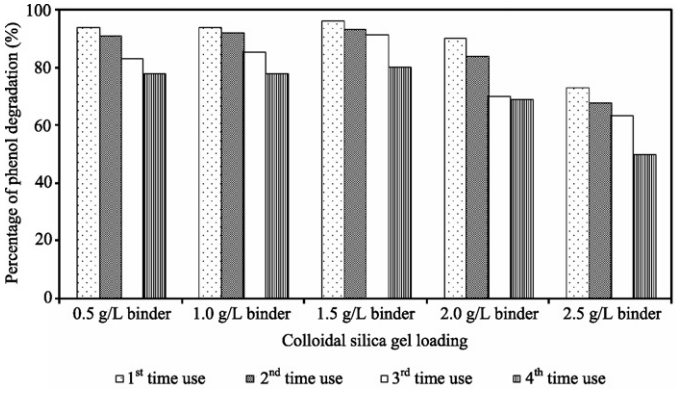

Fig. 9. Comparison of photocatalytic activity of SNTZS catalyst at different loading of binder for four times used, based on the base supported catalyst composition (nano-TiO_2:ZSM-5:silica gel:colloidal silica gel = 1:1:1:2) which 0.25 g TiO_2 was used in 500 mL phenol (0.5 g/L, TiO_2). *Conditions*: Air flow rate = 2 L/min, initial phenol concentration = 50 mg/L).

the highest for 1.5 g/L compared to other colloidal silica gel loadings. However, the reusability of the SNTZS catalyst with 0.5 and 1.0 g/L colloidal silica gel can almost execute as well as that with 1.5 g/L colloidal silica gel. Nevertheless, an increase in the binder amount beyond that limit caused the decrease in the photocatalytic activity. Since the result revealed that the photocatalytic activity among 0.5–1.5 g/L of colloidal silica gel slightly differed from each other, 0.5 g/L was chosen as an essential aspect of the cost effectiveness. The percentage degradation of 0.5 g/L colloidal silica gel decreased to 91% when it was used for a second time compared to 94% when it was firstly used. The percentage degradation of phenol decreased to about 18% when it was used for the fourth time. These results revealed that this binder could maintain the adhesion of the catalyst over an extended period of time, without losing of the photocatalytic activity.

As mention in Sections 3.3.1–3.3.3, the optimum amount of TiO_2 loading is found to be 0.5 g/L for phenol degradation, while the optimum loading of ZSM-5 and support are both concluded at 0.3 g/L. The optimum loading amount of each component was determined after taking into consideration the aspects of percentage phenol degradation and economic effect. For the colloidal silica gel loading effect, the optimum loading was also determined based on the stability of the catalyst for repeated usage without losing its photocatalytic activity. Since the performance of 0.5 g/L colloidal silica gel is not much differs from 1.0 g/L and 1.5 g/L colloidal silica gel, 0.5 g/L colloidal silica gel is chosen as the optimum loading and this is what the author means by considering economic effect. As a result, the optimum composition of the SNTZS is found to be (nano-TiO_2:ZSM-5:silica gel:colloidal silica gel = 1:0.6:0.6:1) which 0.25 g TiO_2 was used in 500 mL phenol (0.5 g/L TiO_2).

3.4. Photocatalytic activity of SNTZS (optimum composition) compared to commercial Degussa P25

The photocatalytic performance of commercial Degussa P25 was also deliberated as a reference to that of the SNTZS. As can be seen in Fig. 10, the optimum composition of SNTZS shows the highest photocatalytic activities compared to the Degussa P25. The optimum supported catalyst composition (nano-TiO_2:ZSM-5:silica gel:colloidal silica gel = 1:0.6:0.6:1) which 0.25 g TiO_2 was used in 500 mL phenol (0.5 g/L TiO_2). Degussa P25 in the amount of 0.25 g TiO_2 was also used in 500 mL phenol (0.5 g/L TiO_2). Boujday et al.

[40] reported that structural and textural properties are important factor involving in the enhancement of the photocatalytic activities. The crystalline quality (structural parameter) that influenced the most in the photocatalysis mechanism includes:

- photon absorption;
- charge-carriers generation;
- charge-carriers migration to the surface;
- charge-carriers trapping.

The SNTZS that consisting of the anatase phase of high crystalline nano-TiO_2 creates a lot of electron–hole pairs with longer lifetimes [40]. The latter was expected to reduce the charge-carriers recombination probability and enhance the photodegradation of phenol. Meanwhile, the specific surface area (textural parameter) influences the interfacial charge transfer. The result of photocatalytic degradation of phenol as shown in Fig. 10 disclosed that an increase in the specific surface area increased the reactivity as well. As mentioned earlier, Al–O units in the zeolite framework were photocatalytic active sites. Thus, this unit did contribute to the enhancement of surface area of the optimum composition of SNTZS (275.7 m^2/g) and hence, resulting better photocatalytic activity compared to the Degussa P25 (50 m^2/g). Besides, the optimum composition of SNTZS has smaller particle size, 8–22 nm (see TEM and XRD result) compared to Degussa P25, 21.3 nm (see TEM result) which in turn showing faster phenol degradation than Degussa P25.

In order to study the reusability of the optimum composition of SNTZS in photodegradation of phenol, the catalyst was repeated for five times. All the procedures of the repeated experimental were same as done in Section 3.3.4. After three experimental runs, the photocatalytic performance of the optimum composition maintained about 90% of phenol degradation (180 min irradiation time), and for the fourth and fifth cycles, the percentage degradation decrease to 88% and 87%, respectively (diagram not shown). Thus, the SNTZS at the optimum composition has revealed to be stable for repeated usage.

4. Conclusions

SNTZS photocatalyst was successfully synthesized using the modified sol–gel method. The performance study of the degradation of phenol over the synthesized photocatalyst under the UV irradiation was performed in a batch reactor. A series of experiments were conducted to investigate the optimum composition for SNTZS. The optimum formulation for the SNTZS which consists of the mixture of nano-TiO_2 and ZSM-5 supported on silica gel using colloidal silica gel as binder was found to be (nano-TiO_2:ZSM-5:silica gel:colloidal silica gel = 1:0.6:0.6:1). About 90% of phenol was degraded after a UV-254 nm irradiation for 180 min over the synthesized SNTZS. Comparatively, the phenol degradation over the Degussa P25 after 180 min was only 67%. After five times of repeated use, the catalyst showed only a slight decrease in the activity. Therefore, the SNTZS synthesized in this study has been proven to have excellent photocatalytic activity and stable for repeated usage. The synthesized SNTZS compared to that of Degussa P25 exhibits superior photocatalytic activity for the photocatalytic degradation of phenol. Its high photocatalytic activity because of the large specific surface area, low electron–hole pairs recombination rate and high crystalline quality of the synthesized catalyst.

Acknowledgements

The authors gratefully acknowledge the Universiti Sains Malaysia and the Ministry of Science, Technology and Innovation Malaysia for funding this project in the form of the USM Research University Grant (1001/PJKIMIA/811068) and the ScienceFund Grant (305/PJKIMIA/6013338), respectively.

References

[1] X. Yang, R. Zou, F. Huo, D. Cai, D. Xiao, Preparation and characterization of Ti/SnO_2–Sb_2O_3–Nb_2O_5/PbO_2 thin film as electrode material for the degradation of phenol, J. Hazard. Mater. 164 (2009) 367–373.
[2] Y.Q. Wang, B. Gu, W.L. Xu, Electro-catalytic degradation of phenol on several metal-oxide anodes, J. Hazard. Mater. 162 (2009) 1159–1164.
[3] Z. Wang, W. Cai, X. Hong, X. Zhao, F. Xu, C. Cai, Photocatalytic degradation of phenol in aqueous nitrogen-doped TiO_2 suspensions with various light sources, Appl. Catal. B 57 (2005) 223–231.
[4] N. Venkatachalam, M. Palanichamy, V. Murugesan, Sol–gel preparation and characterization of alkaline earth metal doped nano TiO_2: efficient photocatalytic degradation of 4-chlorophenol, J. Mol. Catal. A: Chem. 273 (2007) 177–185.
[5] D. Robert, S. Malato, Solar photocatalysis: a clean process for water detoxification, Sci. Total Environ. 291 (2002) 85–97.
[6] L.F. Liotta, M. Gruttadauria, G.D. Carlo, G. Perrini, V. Librando, Heterogeneous catalytic degradation of phenolic substrates: catalysts activity, J. Hazard. Mater. 162 (2009) 588–606.
[7] L. Gomathi Devi, G. Krishnamurthy, TiO_2/$BaTiO_3$-assisted photocatalytic mineralization of diclofop-methyl on UV-light irradiation in the presence of oxidizing agents, J. Hazard. Mater. 162 (2009) 899–905.
[8] H. Yahiro, T. Miyamoto, N. Watanabe, H. Yamaura, Photocatalytic partial oxidation of a-methylstyrene over TiO_2 supported on zeolites, Catal. Today 120 (2007) 158–216.
[9] M.N. Abellán, R. Dillert, J. Giménez, D. Bahnemann, Evaluation of two types of TiO_2-based catalysts by photodegradation of DMSO in aqueous suspension, J. Photochem. Photobiol. A: Chem. 202 (2009) 164–171.
[10] N. Venkatachalam, M. Palanichamy, B. Arabindoo, V. Murugesan, Enhanced photocatalytic degradation of 4-chlorophenol by Zr4+ doped nano TiO_2, J. Mol. Catal. A: Chem. 266 (2007) 158–165.
[11] L.C. Chen, C.M. Huang, F.R. Tsai, Characterization and photocatalytic activity of K^+-doped TiO_2 photocatalysts, J. Mol. Catal. A: Chem. 265 (2007) 133–140.
[12] C. Xie, Z. Xu, Q. Yang, B. Xue, Y. Du, J. Zhang, Enhanced photocatalytic activity of titania–silica mixed oxide prepared via basic hydrolyzation, Mater. Sci. Eng. B 112 (2004) 34–41.
[13] S. Gelover, P. Mondragon, A. Jimenez, Titanium dioxide sol–gel deposited over glass and its application as a photocatalyst for water decontamination, J. Photochem. Photobiol. A: Chem. 165 (2004) 241–246.
[14] Y.M. Wang, S.W. Liu, Z. Xiu, X.B. Jiao, X.P. Cui, J. Pan, Preparation and photocatalytic properties of silica gel-supported TiO_2, Mater. Lett. 60 (2006) 974–978.
[15] F. Haque, E. Vaisman, C.H. Langford, A. Kantzas, Preparation and performance of integrated photocatalyst adsorbent (IPCA) employed to degrade model organic compounds in synthetic wastewater, J. Photochem. Photobiol. A: Chem. 169 (2005) 21–27.
[16] M. Mahalakshmi, S.V. Priya, B. Arabindoo, M. Palanichamy, V. Murugesan, Photocatalytic degradation of aqueous propoxur solution using TiO_2 and Hβ zeolite-supported TiO_2, J. Hazard. Mater. 161 (2009) 336–343.
[17] K. Yamaguchi, K. Inumaru, Y. Oumi, T. Sano, S. Yamanaka, Photocatalytic decomposition of 2-propanol in air by mechanical mixtures of TiO_2 crystalline particles and silicalite adsorbent: the complete conversion of organic molecules strongly adsorbed within zeolitic channels, Micropor. Mesopor. Mater. 117 (2009) 350–355.
[18] K. Tanaka, J. Fukuyoshi, H. Segawa, K. Yoshida, Improved photocatalytic activity of zeolite- and silica-incorporated TiO_2 film, J. Hazard. Mater. 137 (2006) 947–951.
[19] M.V. Shankar, S. Anandan, N. Venkatachalam, B. Arabindoo, V. Murugesan, Fine route for an efficient removal of 2,4-dichlorophenoxyacetic acid (2,4-D) by zeolite supported TiO_2, Chemosphere 63 (2006) 1014–1021.
[20] G. Yan, X. Wang, X. Fu, D. Li, A primary study on the photocatalytic properties of HZSM-5 zeolite, Catal. Today 93–95 (2004) 851–856.
[21] C. Gennequin, M. Lamallem, R. Cousin, S. Siffert, F. Aı¨ssi, A. Aboukaı¨s, Catalytic oxidation of VOCs on Au/Ce-Ti-O, Catal. Today 122 (2007) 301–306.
[22] R.N. Viswananth, S. Ramasamy, Study of TiO_2 nanocrystallites in TiO_2-SiO_2 composites, Colloids Surf. A 133 (1998) 49–56.
[23] S. Bakardjieva, J. Subrt, V. Stengl, M.J. Dianez, M.J. Sayagues, Photoactivity of anatase–rutile TiO_2 nanocrystalline mixtures obtained by heat treatment of homogeneously precipitated anatase, Appl. Catal. B: Environ. 58 (2005) 193–202.
[24] H.C. Liang, X.Z. Li, Effects of structure of anodic TiO_2 nanotube arrays on photocatalytic activity for the degradation of 2,3-dichlorophenol in aqueous solution, J. Hazard. Mater. 162 (2009) 1415–1422.
[25] Q. Xiao, L. Ouyang, Photocatalytic activity and hydroxyl radical formation of carbon-doped TiO_2 nanocrystalline: effect of calcination temperature, Chem. Eng. J. 148 (2009) 248–253.
[26] M.S. Lee, S.S. Hong, M. Mohseni, Synthesis of photocatalytic nanosized TiO_2–Ag particles with sol–gel method using reduction agen, J. Mol. Catal. A: Chem. 242 (2005) 135–140.
[27] L. Wu, J.C. Yu, L. Zhang, X. Wang, W. Ho, Preparation of a highly active nanocrystalline TiO_2 photocatalyst from titanium oxo cluster precursor, J. Solid State Chem. 177 (2004) 2584–2590.

[28] J. Yang, J. Zhang, L. Zhu, S. Chen, Y. Zhang, Y. Tang, Y. Zhu, Y. Li, Synthesis of nano titania particles embedded in mesoporous SBA-15: characterization and photocatalytic activity, J. Hazard. Mater. 137 (2006) 952–958.
[29] A.N. Ökte, O. Yilmaz, Characteristics of lanthanum loaded TiO_2-ZSM-5 photocatalysts: decolorization and degradation processes of methyl orange, Appl. Catal. A: Gen. 354 (2009) 132–142.
[30] S. Brunauer, P.H. Emmer, E. Teller, Adsorption of gases in multimolecular layers, J. Am. Chem. Soc. 60 (1938) 309–319.
[31] X. Fan, X. Chen, S. Zhu, Z. Li, T. Yu, J. Ye, Z. Zou, The structural, physical and photocatalytic properties of the mesoporous Cr-doped TiO_2, J. Mol. Catal. A: Chem. 284 (2008) 155–160.
[32] L. Wei, C. Shifu, Z. Wei, Z. Sujuan, Titanium dioxide mediated photocatalytic degradation of methamidophos in aqueous phase, J. Hazard. Mater. 164 (2009) 154–160.
[33] H.R. Pouretedal, A. Norozi, M.H. Keshavarz, A. Semnani, Nanoparticles of zinc sulfide doped with manganese, nickel and copper as nanophotocatalyst in the degradation of organic dyes, J. Hazard. Mater. 162 (2009) 674–681.
[34] P.S. Awati, S.V. Awate, P.P. Shah, V. Ramaswamy, Photocatalytic decomposition of methylene blue using nanocrystalline anatase titania prepared by ultrasonic technique, Catal. Commun. 4 (2003) 393–400.
[35] M. Inagaki, R. Nonaka, B. Tryba, A.W. Morawski, Dependence of photocatalytic activity of anatase powders on their crystallinity, Chemosphere 64 (2006) 437–445.
[36] K.V. Baiju, S. Shukla, K.S. Sandhya, J. James, K.G.K. Warrier, Photocatalytic activity of sol–gel-derived nanocrystalline titania, J. Phys. Chem. C 111 (2007) 7612–7622.
[37] S. Banerjee, J. Gopal, P. Muraleedharan, A.K. Tyagi, B. Raj, Physics and chemistry of photocatalytic titanium dioxide: visualization of bactericidal activity using atomic force microscopy, Current Sci. 90 (2006) 1378–1383.
[38] H.K. Singh, M. Saquib, M.M. Haque, M. Muneer, D.W. Bahnemann, Titanium dioxide mediated photocatalysed degradation of phenoxyacetic acid and 2,4,5-trichlorophenoxyacetic acid, in aqueous suspensions, J. Mol. Catal. A: Chem. 264 (2007) 66–72.
[39] M. Tasbihi, C.R. Ngah, N. Aziz, A. Mansor, A.Z. Abdullah, K.T. Lee, A.R. Mohamed, Lifetime and regeneration studies of various supported TiO_2 photocatalysts for the degradation of phenol under UV-C light in a batch reactor, Ind. Eng. Chem. Res. 46 (2007) 9006–9014.
[40] S. Boujday, F. Wunsch, P. Portes, J.F. Bocquet, C. Colbeau-Justin, Photocatalytic and electronic properties of TiO_2 powders elaborated by sol–gel route and supercritical drying, Sol. Energy Mater. Sol. Cells 83 (2004) 421–433.